

1995120930

N95-27351

465367

TRANSIENT STUDIES OF G-INDUCED CAPILLARY DRYOUT AND REWET

M.K. Reagan and W.J. Bowman
Department of Aeronautics and Astronautics
Air Force Institute of Technology
Wright Patterson Air Force Base, Ohio

56-34
~~45099~~
p. 22

SUMMARY

A transient, one-dimensional numerical code is developed to model the liquid motion in an axial groove with square cross section. Axial variation in liquid level, shear stress and heat transfer between the groove wall and the liquid, evaporation and transient body forces are accounted for in the model. Dryout and rewet of the groove are allowed; the front location is determined numerically using conservation of mass and linear extrapolation. Several numerical test results are presented and discussed.

INTRODUCTION

Heat pipe technology has been proposed for use in the aerospace environment as a means of cooling electronics on fighter aircraft or as a means of thermal management aboard space-based platforms (refs. 1-3). These environments are dynamic ones where time-varying body forces will primarily influence the motion of the working fluid within the wick structure of the heat pipe. While the magnitudes of the body forces in these two examples may be quite different, the effect on the working fluid in the wick is the same; namely, a bulk movement of the fluid towards either the evaporator or the condenser, depending on the magnitude and orientation of the body force. If the bulk motion of the fluid is towards the condenser, then dryout of the wick structure will be enhanced and heat pipe failure will result. The ability to correctly model liquid motion in a wick structure subject to transient body forces, then, is a necessary first step before heat pipe technology will be accepted as a means of thermal management in the aerospace industry.

Several attempts have been made to numerically model the liquid flow in a heat pipe wick. Two models repeatedly found in the literature are the Groove Analysis Program (GAP), developed by NASA (ref. 4) and a piston model developed by Beam (ref. 5). GAP is a steady-state formulation that is applicable only to grooved wick structures. Because it is steady-state, it does not account for the time-varying nature of body forces. It properly models the axial variation in radius of curvature; however, this radius of curvature is only allowed to vary from a minimum at the evaporator (equal to one-half the groove width) to a maximum at the condenser (equal to the radius of the vapor space). Because of this, dryout is never allowed to occur and therefore, it provides no capability to predict or model the dryout and rewet phenomena.

The piston model of Beam; however, is an unsteady formulation that does account for transient body forces. The wick is assumed to be entirely full up to the dryout front, past which no liquid may be present. The front is perpendicular to the axial direction, hence the reference to a piston. Because the

wick is assumed to be entirely full up to the front location, no recession of liquid and therefore, no radius of curvature, is allowed axially along the wet portion of the wick. In an actual heat pipe, recession of the liquid into the wick structure occurs continuously between the evaporator and condenser without causing dryout and always occurs as a precursor to dryout. Visual observations of Reagan (ref. 6) and Hawthorne (ref. 7) have verified this behavior. Because no liquid recession into the wick is allowed, the piston model predicts dryout earlier than actually occurs.

A limitation of both models is that neither attempts to describe the nature or behavior of the liquid front within the wick. In the GAP model, no liquid front is allowed to develop; the simulations are stopped when the capillary limit is reached. In the piston model, the front is treated like a piston with no attempt to describe what it actually looks like.

Additionally, both models assume that momentum changes in the liquid are negligible. This reduces the momentum equation to a form of Darcy flow, which models the pressure drop by equating the sum of pressure, shear and body force terms to zero and neglects any change in the liquid inertia. During steady-state behavior, the liquid velocity is small and hence, inertia effects are most likely negligible. The same conclusion cannot be deduced for the case of a transient body force environment. A new transient numerical model is therefore warranted.

THEORY

Several assumptions are made concerning the derivation of the governing equations. The wick is an axial groove with square cross section of constant width, w and depth, δ . One end of the groove can be tilted relative to the other end which provides the transient body force. No flooding of the groove is allowed and the pressure above the liquid in the groove is assumed constant and equal to ambient pressure, P_∞ .

The working liquid is ethanol and is assumed to be incompressible with density, $\rho = 785 \text{ kg/m}^3$. Laminar flow within the groove is assumed at all times and kinetic and potential energy changes are assumed negligible with respect to changes in the internal energy. Free convection and radiation losses to the environment are also considered negligible with respect to the energy lost via evaporation.

Consider the control volume shown in Figure 1. This control volume encompasses the liquid only and not the groove structure. The liquid flow is from left to right and the meniscus level is assumed to vary linearly through the control volume. The equation of conservation of mass for this control volume, noting that ρdx is constant, yields

$$\frac{\partial A}{\partial t} + \frac{\partial(AV)}{\partial x} + \frac{\dot{m}_e}{\rho dx} = 0 \quad (1)$$

where A is the liquid cross-sectional flow area, V is the average liquid velocity and \dot{m}_e is the evaporative mass flow rate for the differential control volume.

Figure 2 shows the same control volume with the appropriate forces (solid arrows) and momentum terms (dashed arrows). The groove with the liquid is tilted at an angle, ψ , around a center of rotation relative to the horizontal level and this angle is a function of time, which provides the transient body force, $\rho Ag \sin \psi dx$ ($g = \text{gravitational constant}$). Momentum changes within the liquid, evaporative momentum flux, shear and capillary forces are all accounted for. The meniscus radius of curvature, R ,

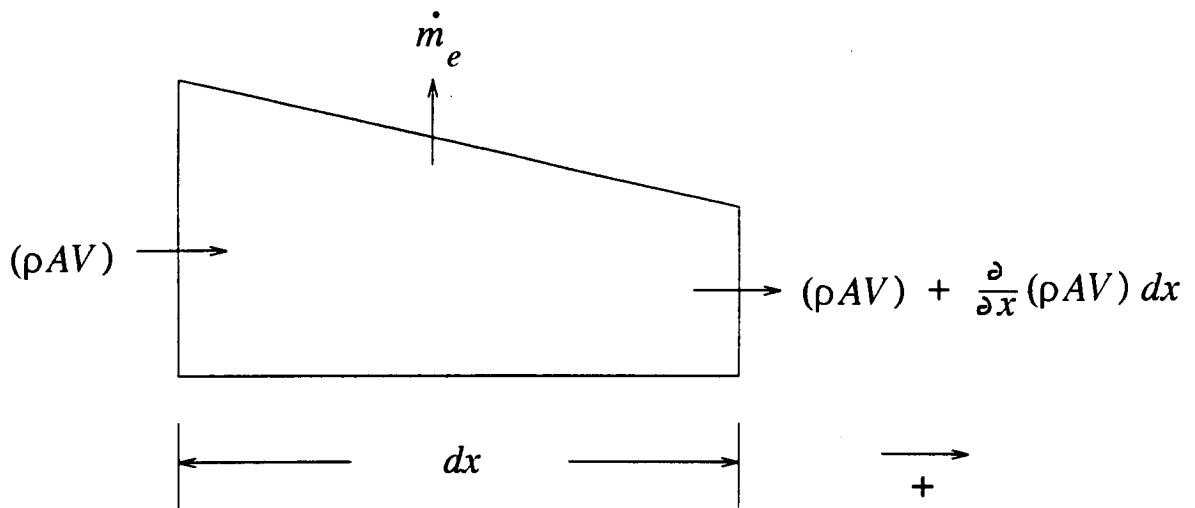


Figure 1. Control Volume for Conservation of Mass Analysis

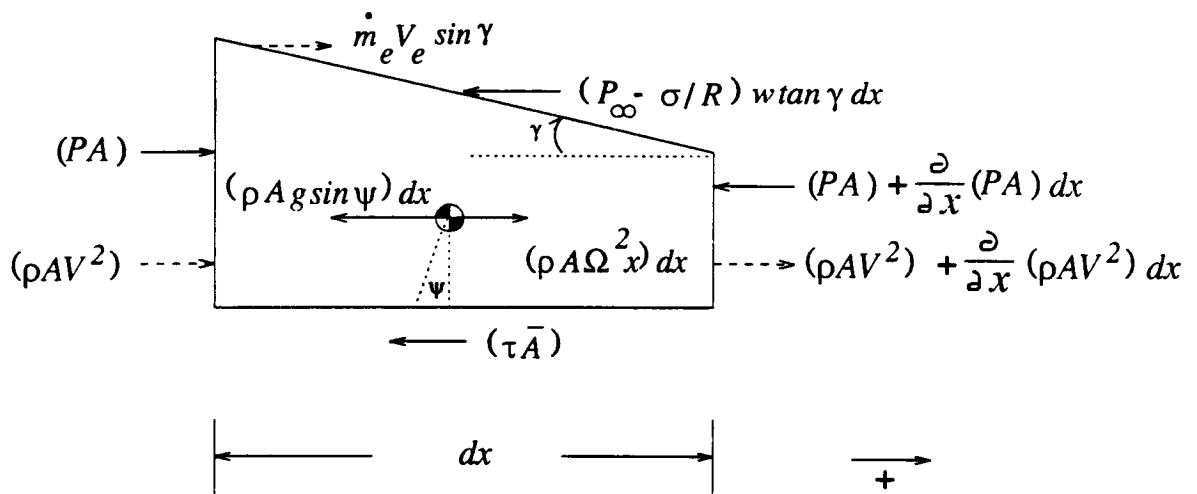


Figure 2. Control Volume for Conservation of Momentum Analysis

is a function of the liquid cross-sectional flow area and therefore can vary with axial location. The $(\rho A \Omega^2 x) dx$ term is a fictitious force term which accounts for the non-inertial reference frame of the governing equations. Applying conservation of momentum to this control volume yields

$$\frac{\partial(AV)}{\partial t} + \frac{\partial}{\partial x} \left(AV^2 + \frac{PA}{\rho} \right) = \frac{\dot{m}_e V_e \sin \gamma}{\rho dx} - Ag \sin \psi - \frac{\tau \bar{A}}{\rho dx} - \frac{1}{\rho} \left(P_\infty - \frac{\sigma}{R} \right) w \tan \gamma + A \Omega^2 x \quad (2)$$

where γ is the angle generated by the axial variation in meniscus level, V_e is the evaporative mass flux velocity, τ is the shear stress between the groove wall and liquid, \bar{A} is the area over which the shear stress acts, σ is the surface tension coefficient and Ω is the angular rotation rate.

The average liquid pressure, P , at any axial location is assumed to be the ambient pressure minus the capillary pressure due to the curved interface, plus the pressure head due to the depth of liquid in the groove. The average depth of liquid in the groove, h , is approximated by $h = A/w$, and the average pressure head can be shown to be $\frac{1}{2} \rho g h \cos \psi$. The average liquid pressure then, is a function of the groove tilt angle, ψ , the cross-sectional flow area, A , and the meniscus radius of curvature, R .

This meniscus radius of curvature is a function of the liquid cross-sectional flow area and is assumed to behave as shown in Figure 3. When the groove is entirely full of liquid, there is no meniscus and the radius of curvature is infinite. As liquid evaporates or is moved by bulk motion, the meniscus recedes into the groove and R decreases from infinity until a hemispherical shape is formed. The radius of curvature at this condition is $R = w/2$. This hemispherical shape remains constant until the tangent to the meniscus is coincident with the bottom of the groove. As more liquid is removed by bulk motion or evaporation, the meniscus recedes further into the corners of the groove and the radius of curvature continues to decrease. This decrease is allowed to continue until the resulting liquid pressure is zero--a physical limitation. These three conditions (entirely full, initial hemisphere shape and tangent condition) allow a mathematical relationship between the cross-sectional flow area and the radius of curvature to be derived. Details of this derivation are found in Reference 6.

The shear stress between the groove wall and the liquid, τ , is modeled using

$$\tau = \frac{f \rho V^2}{2} \quad (3)$$

where the friction coefficient, f , is determined using rectangular tube flow data from Shah (ref. 8) and modified for channel flow according to Chi (ref. 9). The remaining quantities in Eqn (2) (evaporative mass flux, groove tilt angle and angular rotation) are assumed to be known or measurable quantities.

The energy equation for this system is derived using the control volume in Figure 4. The total energy per unit mass is approximated by the internal energy, $E \approx e = c_p T$, where c_p is the liquid specific heat and T is the bulk liquid temperature. The energy influx, Q_{in} , is modeled using Newton's Law $Q_{in} = h_{in} A_{in} (T_g - T)$, where A_{in} is the groove wall area across which the heat energy travels, T_g is the groove wall temperature which is assumed known or measurable, and h_{in} is the transfer coefficient. This coefficient was calculated using

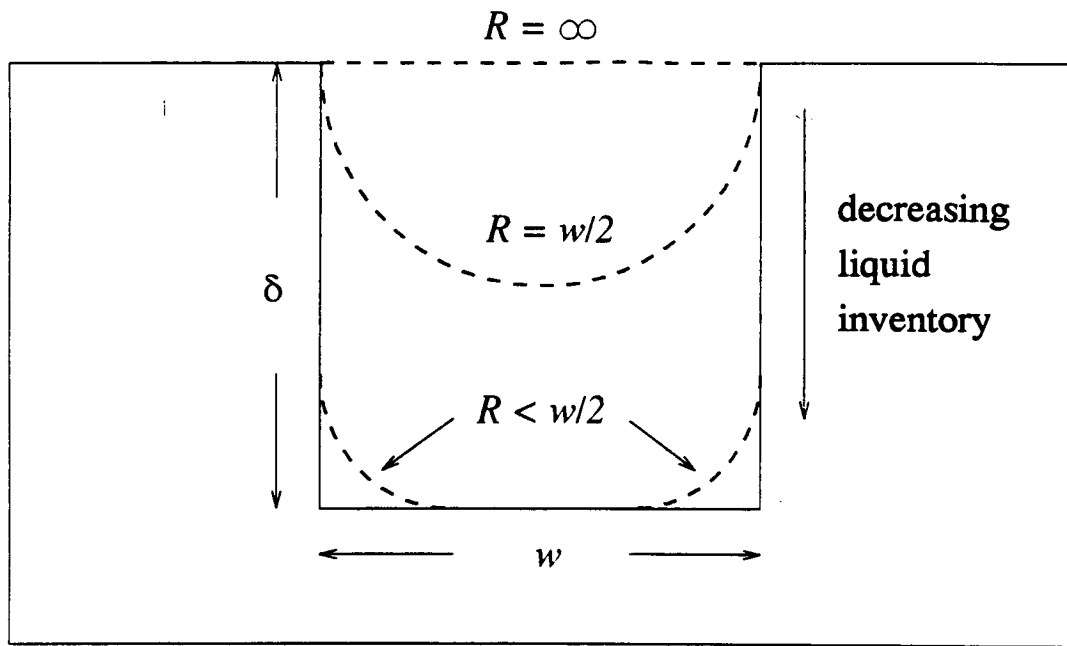


Figure 3. Meniscus Behavior in a Square Groove

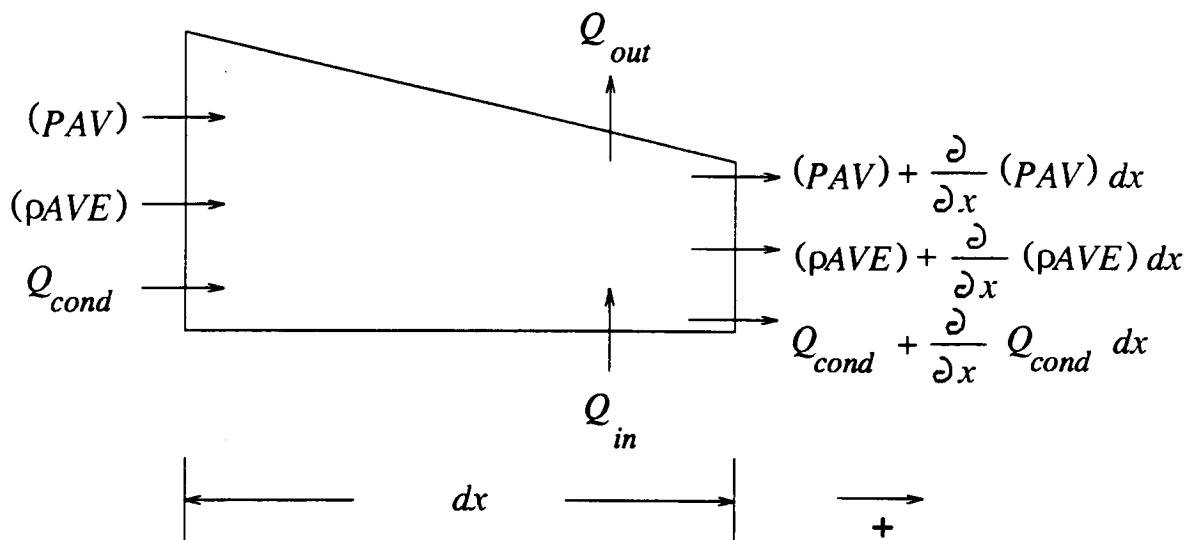


Figure 4. Control Volume for Conservation of Energy Analysis

$$h_{in} = \frac{Nu k}{D_h} \quad (4)$$

where Nu is the Nusselt Number, k is the liquid thermal conductivity and D_h is the hydraulic diameter. Nu was determined using convection correlations for constant surface heat flux (ref. 10), laminar tube flow and corrected for channel flow similar to the method used for the friction coefficient (see ref. 6 for more information).

The energy outflow, Q_{out} , is determined using $Q_{out} = \dot{m}_e \lambda$, where λ is the latent heat of vaporization. Q_{cond} is the rate of energy conducted axially through the control volume and was calculated using Fourier's Conduction Law. Applying these definitions, the energy equation for this control volume is written as

$$\frac{\partial}{\partial t}(AE) + \frac{\partial}{\partial x} \left(AV \left[E + \frac{P}{\rho} \right] \right) = \frac{(Q_{in} - Q_{out})}{\rho dx} - \frac{1}{\rho} \frac{\partial Q_{cond}}{\partial x} \quad (5)$$

Eqns (1), (2) and (5) form the set of governing equations for the new model. The pressure-area and radius-area relationships discussed previously provide closure for the system. The temporal derivative terms are grouped into a 3×1 matrix, \bar{U} , and the spatial derivative terms are grouped into a 3×1 matrix, \bar{E} . The remaining terms are combined into a source term, \bar{S} and the resulting system is written as

$$\bar{U}_t + \bar{E}_x = \bar{S} \quad (6)$$

where the subscripts t and x refer to time and space derivatives respectively. Eqn (6) is non-dimensionalized and integrated using a first order accurate, explicit Roe scheme. Details of the solution methodology are found in Reference 6.

BOUNDARY CONDITIONS

The integration is performed on a one-dimensional grid, GRID1, that is I nodes wide as shown in Figure 5. Node 1 lies on the left boundary; this node is also the center of rotation of the groove. As such, it always contains liquid and because of the physical boundary, the velocity is always zero. The grid extends to I nodes, some or all of which have liquid in them, depending on the dryout/rewet front location. Node nb refers to the last wet node and is only equal to node I if the groove is fully wet. The grid remains fixed to the groove structure and does not move with the liquid.

At time level n , the total mass of liquid in the groove, m_g , is known. At time level $n+1$, assuming mass loss only by evaporation, the total mass of liquid in the groove is

$$m_g^{n+1} = m_g^n - \sum_{i=2}^{nb} \dot{m}_e \Delta t \quad (7)$$

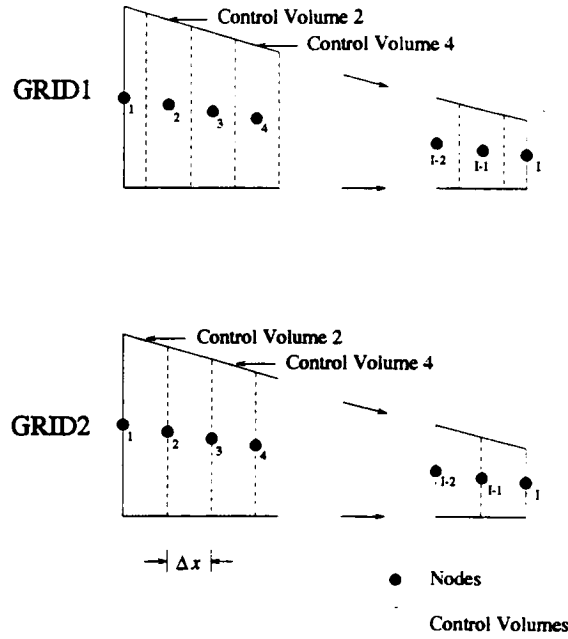


Figure 5. Numerical Grid Definitions

A second grid, GRID2, is used to update the boundary conditions and is also shown in Figure 5. The mass within any control volume using this grid is found using

$$m_i^n = \frac{1}{2} \rho \Delta x (A_i^n + A_{i-1}^n) \quad (8)$$

and the internal mass, m_{int} , is calculated by summing m_i^n between volumes 3 and nb . Applying the principle of conservation of mass to the leftmost control volume of GRID2 yields the area of node 1 as

$$m_2^{n+1} = m_2^n - \Delta t (\dot{m}_2^n + \dot{m}_e^n) \quad (9)$$

$$\Rightarrow A_1^{n+1} = \frac{2m_2^{n+1}}{\rho \Delta x} - A_2^{n+1}$$

The velocity at node 1 is zero because of the physical boundary and the temperature is updated assuming an adiabatic end condition.

The remaining mass in the groove, m_r , at time level $n+1$ is found by subtracting the internal mass and the mass at node 2 calculated in Eqn (9) above from the predicted mass at time level $n+1$ (Eqn (7))

$$m_r^{n+1} = m_g^{n+1} - m_{int}^{n+1} - m_2^{n+1} \quad (10)$$

If the groove is not in a state of dryout, then m_r occupies control volume I and the area at node I is found by a simple average of the areas at nodes I and I-1. The velocity at node I is identically zero and the temperature is updated assuming an adiabatic end condition.

If, however, the groove is in a state of dryout or rewet, then a front exists and m_r occupies some specified volume extending beyond node nb . Several possibilities exist regarding the distribution of liquid extending beyond this node. Two of the more obvious are seen in Figure 6. The first order approximation fills a right triangle with the remaining mass, while the second order approximation attempts to match the remaining mass to a parabola with a specified slope at the front location. Higher order matches are also possible. For this work, the first order approximation is used.

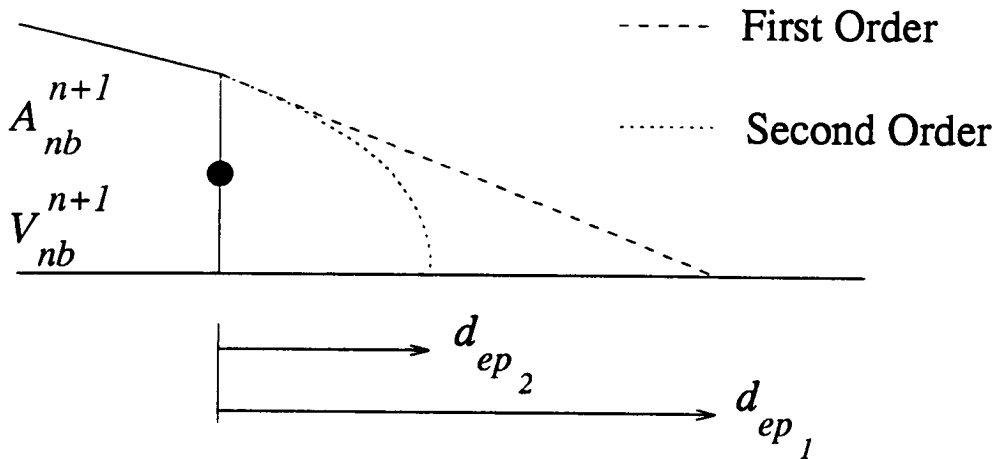


Figure 6. Sample Front Approximations

Defining the location in the groove where the cross-sectional flow area goes to zero as the extinction point, ep , then the distance between node nb and the extinction point is

$$d_{ep} = \frac{2m_r^{n+1}}{\rho A_{nb}^{n+1}} \quad (11)$$

This length can extend to one or to several nodes beyond node nb or it may not even extend to node $nb+1$ depending on the magnitude of m_r . Regardless, the boundary conditions at the extinction point are defined by the following relationships

Figure 8 shows the results of a ten second real time computer run. This is a three-dimensional plot of the non-dimensional area distribution in the groove, A^* , as a function of non-dimensional time, t^* , and non-dimensional axial groove location, x^* . Each axis runs from a minimum value of zero to a maximum value of one. The perspective of the liquid distribution is from an observer positioned on the groove. According to the figure, the area distribution does not vary with time from its initial level value of 0.5 (one-half full); the steady-state condition.

Test Two--Steady Body Force

This test was accomplished similarly to the first test; the only difference being in the initial groove angle and liquid distribution. The groove is set at an initial angle of, $\psi_{init} = \tan^{-1}(\delta/L_\infty)$, and the initial distribution of liquid is such that $A^* = 1$ at the left end of the groove ($x^* = 0$) and $A^* = 0$ at the right end ($x^* = 1$) with a linear distribution in between, as shown in Figure 9. This provides the same volume of liquid used in the first test. In the absence of any capillary or body forces, there should be no tendency for the liquid to change from this position, which is the steady-state solution for the initial conditions.

Figure 10 shows the results of a ten second real time computer run and reveals no change from the initial distribution described above. This result demonstrates that the hydrostatic and atmospheric pressure forces, along with the body force, are modeled properly and coded correctly.

Test Three--Steady Body Force With Motion

It was necessary to determine if the code could predict the correct steady-state solution for an initial condition other than steady-state. To demonstrate this behavior, a setup identical to test two was used with the initial liquid distribution similar to that of test one and is shown in Figure 11. From this initial condition, the liquid should begin to flow towards the left end of the groove ($x^* = 0$) and reach the steady-state conditions of test two.

Figure 12 shows the results of a ten second real time computer run. Note that as time progresses, A^* increases at $x^* = 0$ and decreases at $x^* = 1$. This shows bulk liquid motion towards $x^* = 0$, and at $t^* = 1$, steady-state conditions are achieved. This test demonstrates that the code predicts the correct steady-state solution for a non steady-state initial condition.

Test Four--Steady Body and Capillary Forces

This test was performed to determine if the capillary force was modeled and coded properly. The initial conditions for this experiment are seen in Figure 13. The groove tilt angle was similar to test three and the liquid distribution was the same as test two. In the absence of the capillary force, it was seen in test two that the liquid had no tendency to move. However, if the capillary force is now considered, the liquid should have a tendency to move towards $x^* = 1$ since the liquid in that end has receded further into the groove and the capillary influence should be greatest.

Figure 14 shows the results from this study. With the capillary force present, the liquid does indeed move towards $x^* = 1$ as seen by the increase in A^* at $x^* = 1$ and a corresponding decrease in A^* at the other end of the groove, $x^* = 0$. The liquid approaches a steady-state distribution different from the steady-state condition seen in Figure 10. This is due to the inclusion of the capillary force.

$$A_{ep} = 0$$

$$\left| \frac{\partial A}{\partial x} \right|_{ep} = \frac{-\rho (A_{nb}^{n+1})^2}{2m_r^{n+1}} \quad (12)$$

If d_{ep} is less than Δx , then m_r is not sufficient to extend the triangular profile to the node $nb+1$. In this case, the area, velocity and temperature distributions of the liquid are completely defined and no further calculations are required.

If, however, d_{ep} is greater than Δx , then the remaining mass is sufficient to extend the profile to node $nb+1$. In this case, A_{nb+1}^{n+1} is calculated using the area at node nb and the slope from Eqn (12). Applying conservation of mass on the control volume between nodes nb and $nb+1$ yields the velocity as

$$V_{nb+1}^{n+1} = \frac{(AV)_{nb}^{n+1} - \left(\frac{\partial \nabla}{\partial t} \right)_{nb+1} - \frac{\dot{m}_e}{\rho}}{A_{nb+1}^{n+1}} \quad (13)$$

where ∇ is the volume of the differential element. A first order approximation to the volume derivative term is used and the evaporation term is evaluated at the temperature of node nb at time level $n+1$. The temperature is updated assuming no axial conduction.

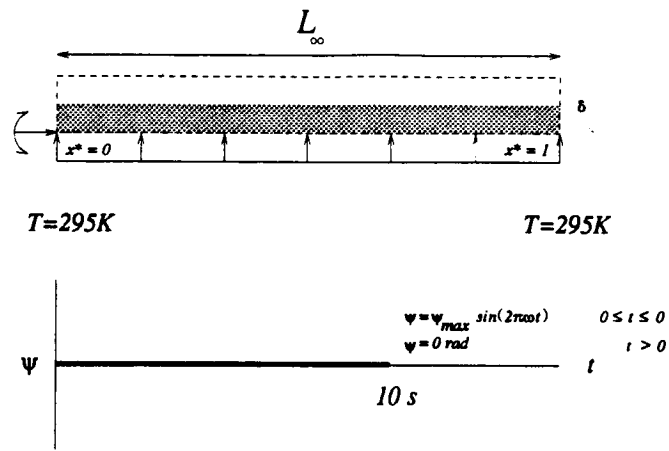
After the area, velocity and temperatures are updated, the mass in the new control volume is calculated and subtracted from m_r and a new m_r is established. Node $nb+1$ is renumbered as node nb and a new value of d_{ep} is calculated and established. The procedure described above is repeated until this new value of d_{ep} is less than Δx .

NUMERICAL TEST PARAMETERS AND RESULTS

Several numerical experiments were performed with the new model to establish confidence in its ability to model the flow of liquid in a heated capillary structure subject to transient body forces. Since no comparisons to physical data are made, absolute accuracy of the results is not considered important. However, correct trends need to be demonstrated as well as the ability to numerically model the formation of a front in the groove structure.

Test One--No Body Force

The purpose of this test was to demonstrate that liquid in a groove that is initially level and remains level should have no tendency to move. The test setup is shown in Figure 7. The groove, shown by the dotted line in the figure, is a square channel. The width, w , and depth, δ , are 1.5875 mm, where the width dimension is into the page. The groove length, L_∞ , is 0.254 m, the liquid is ethanol and the capillary force and evaporation are neglected. In this test, the groove is maintained at the ambient temperature, $T = 295K$, and is not allowed to rotate. The initial area distribution is such that the groove is exactly one-half full. This is represented by the shaded area in the figure.



Run Parameters

$\Psi_{init} = 0 \text{ rad}$	$\sigma = \text{off}$	$t_\infty = 10 \text{ s}$
$\Psi_{max} = 0 \text{ rad}$	$\dot{m}_e = \text{off}$	$L_\infty = 0.254 \text{ m}$
$\omega = 0 \text{ Hz}$		

Figure 7. Numerical Test One Parameters

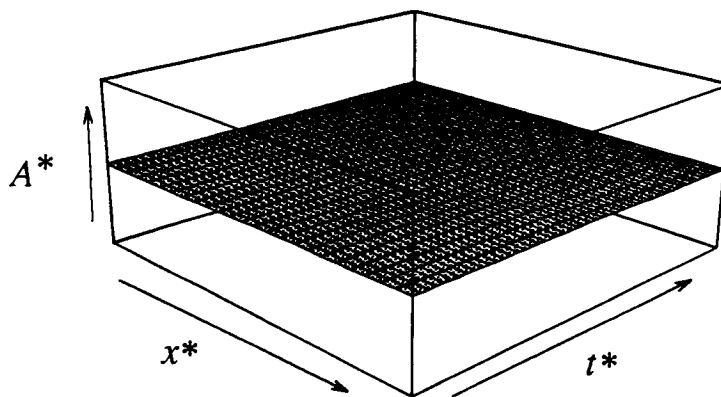
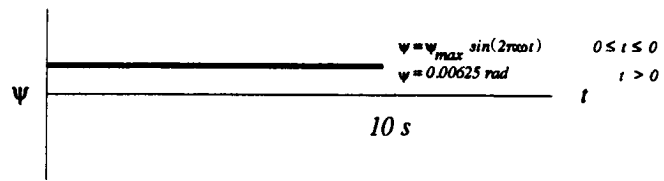
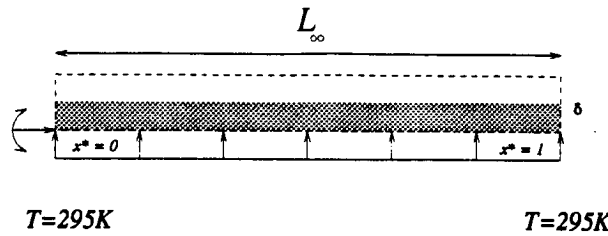


Figure 8. Numerical Test One Results



Run Parameters

$\Psi_{init} = 0.00625 \text{ rad}$	$\sigma = \text{off}$	$t_\infty = 10 \text{ s}$
$\Psi_{max} = 0 \text{ rad}$	$\dot{m}_e = \text{off}$	$L_\infty = 0.254 \text{ m}$
$\omega = 0 \text{ Hz}$		

Figure 11. Numerical Test Three Parameters

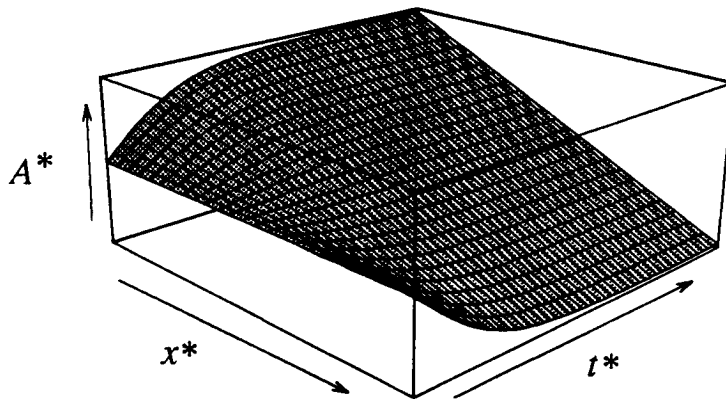
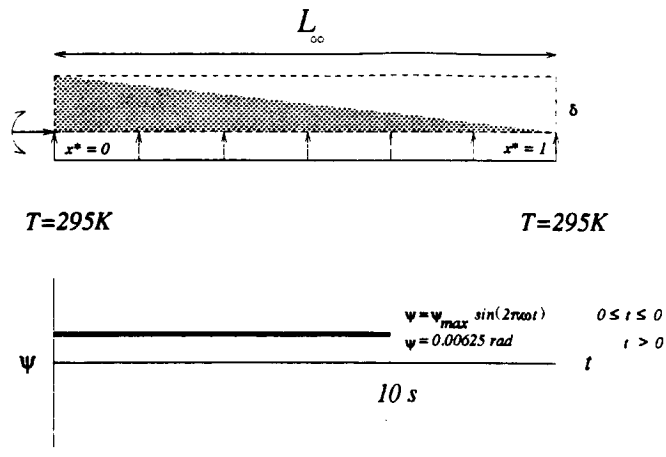


Figure 12. Numerical Test Three Results



Run Parameters

$\Psi_{init} = 0.00625 \text{ rad}$	$\sigma = \text{off}$	$t_\infty = 10 \text{ s}$
$\Psi_{max} = 0 \text{ rad}$	$m_e = \text{off}$	$L_\infty = 0.254 \text{ m}$
$\omega = 0 \text{ Hz}$		

Figure 9. Numerical Test Two Parameters

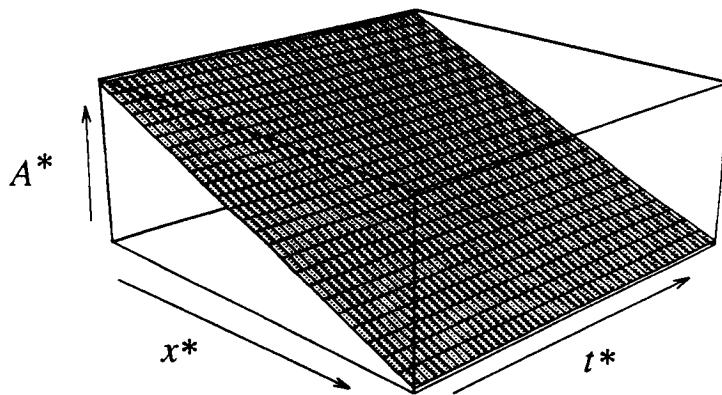
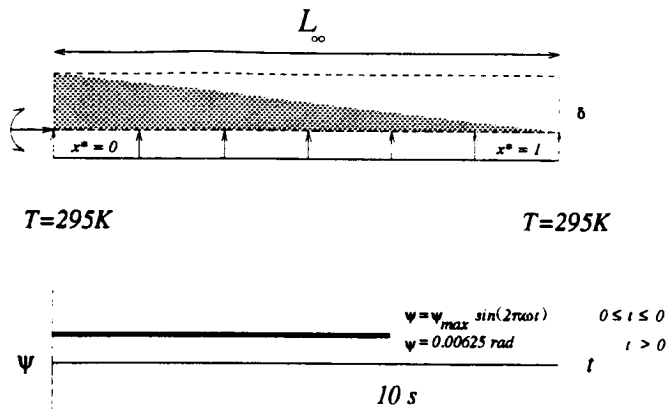


Figure 10. Numerical Test Two Results



Run Parameters

$\Psi_{init} = 0.00625 \text{ rad}$	$\sigma = on$	$t_\infty = 10 \text{ s}$
$\Psi_{max} = 0 \text{ rad}$	$\dot{m}_e = off$	$L_\infty = 0.254 \text{ m}$
$\omega = 0 \text{ Hz}$		

Figure 13. Numerical Test Four Parameters

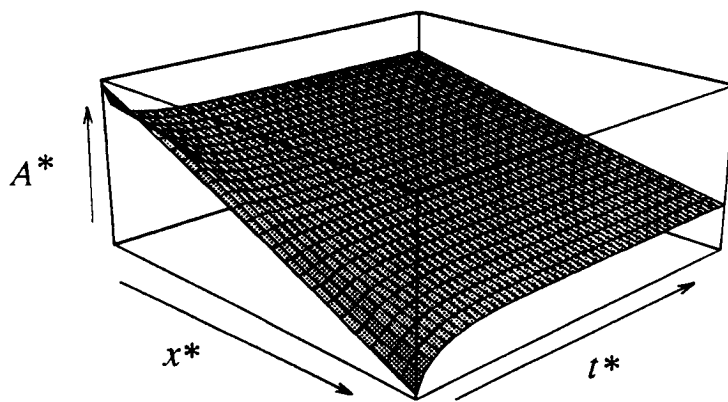


Figure 14. Numerical Test Four Results

The remaining three numerical experiments were performed with the capillary force and evaporation present. The goal of these remaining experiments was to determine the code's ability to model the liquid motion in the groove under transient body forces and external heating; two important parameters that were neglected in tests one through four. The magnitude and duration of the body forces and heating were sufficient to result in dryout in the groove: a phenomenon also not studied in tests one through four.

Test Five--Transient Body Force, No External Heating

This test was performed to determine if the code could capture the formation of a dryout front in a groove that was subject to a transient body force but no external heating. No external heating refers to no externally applied heat sources, such as a heater. It does not mean that no heat transfer takes place; in fact, heat transfer does occur in the form of evaporation.

In this test, the groove was initially at a level condition and one-third full of liquid. The groove was rotated through the schedule shown by the bold line in Figure 15. This schedule was

$$\begin{aligned} \psi &= \psi_{max} \sin(2\pi\omega t) & 0 \leq t \leq 5 \\ \psi &= 0 & t > 5 \end{aligned}$$

with a maximum angle, ψ_{max} , of 0.0524 radians and a frequency of $\omega = 0.1$ Hz. This particular schedule was chosen after numerous numerical test runs because it resulted in a partial dryout of the groove followed by a rewet. The results of this test run are shown in Figure 16. As the transient body force is applied, the level of liquid at $x^* = 0$ increases and the level at $x^* = 1$ decreases, indicating bulk liquid motion towards $x^* = 0$. At approximately $t^* = 0.3$, the groove begins to dry out as noted by $A^* = 0$ at $x^* = 1$. As the tilt schedule reverses direction back towards the initial level condition, the liquid motion follows and the rewet is captured by the increase in A^* from its zero value. At $t^* = 1$, the liquid distribution in the groove is not level as steady-state conditions would dictate. The code was allowed to run for additional time and the liquid distribution did eventually reach a quasi-steady-state condition. This quasi-steady-state refers to the liquid level in the groove being uniform along its length but decreasing in time due to evaporation of the liquid. The time shown in Figure 16 was chosen to reveal details of the dryout and rewet. This experiment validated the code's ability to capture a dryout and rewet due solely to a transient body force.

Test Six--No Body Force, External Heating

This test was performed to determine if the code could capture the formation of a liquid front in a groove subjected to external heating but no transient body force. In this test, the groove was initially at a level condition and entirely full of liquid. The groove was kept level throughout the test as shown in Figure 17. The left end of the groove was maintained at $T = 295K$, while the right end was maintained at $T = 345K$, with a linear distribution of temperature between $x^* = 0$ and $x^* = 1$. A maximum temperature of 345 K was chosen to remain below the boiling point of ethanol. This test was carried out for 480 seconds. For the first 420 seconds, the temperature profile described above was used.

This was done to generate a dry region in the groove. Between 420 and 480 seconds, the temperature profile was reduced to a uniform temperature of $T = 295\text{ K}$ to allow a rewet to occur.

The results of this experiment are seen in Figure 18. Several interesting trends are seen in this figure. First, the decrease in liquid volume between $t^* = 0$ and $t^* = 1$ is evident by the decrease in A^* along the groove. Note however, that the rate of decrease in A^* is greater at $x^* = 1$ than at $x^* = 0$. This is due to the elevated temperatures as x^* approaches one. Higher temperatures result in higher evaporation rates and a quicker depletion of liquid from the groove.

The second trend is the formation of a dryout front, $A^* = 0$, at approximately $t^* = 0.9$. At this point, the elevated temperature profile was reduced to the uniform profile and a rewet of the groove was noted. At $t^* = 1$ the liquid has not reached its quasi-steady-state condition. This test validated the code's ability to capture a dryout and rewet due solely to external heating.

Test Seven--Transient Body Force, External Heating

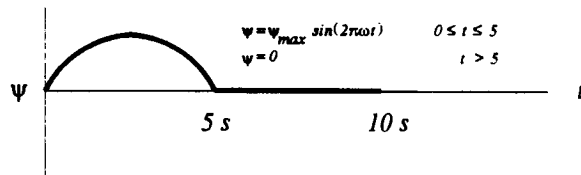
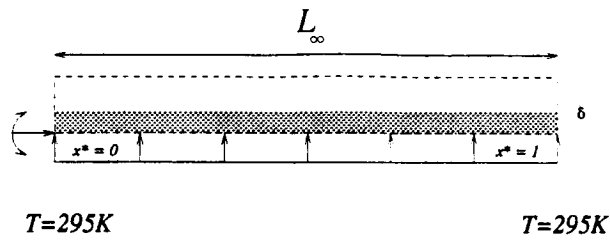
This numerical experiment was performed to determine the code's ability to capture a dryout and rewet in a groove subject to both transient body forces and external heating; similar to what was investigated in the physical experiments. The test setup is shown in Figure 19. The heating schedule of test six was combined with the tilt schedule of test five. The total run time for this experiment was ten seconds. This was done to compare the results to those of test five.

The results are seen in Figure 20. The same trends noted in Figure 16 are seen here; namely, the dryout of the groove at approximately $t^* = 0.3$ and the rewet following the groove rotation back to level. The primary difference between these two figures is in the rewet phase. In Figure 16 the rewet is seen by the rise in A^* at $x^* = 1$ between $t^* = 0.5$ and $t^* = 1$. The same region in Figure 20, however, shows a dryout condition; in fact, at $x^* = 1$, A^* is zero at $t^* = 1$, compared to $A^* = 0.045$ in Figure 16. This is due to the elevated temperatures and correspondingly increased evaporation rates.

Test Eight--Increased Frequency

An additional numerical study was performed to demonstrate the ability of the code to model the liquid flow in a heated capillary structure under a frequency and amplitude greater than those of tests one through seven. The code was run at the same conditions as numerical experiments one through seven, but the amplitude was allowed to vary between $+0.0524$ and -0.0524 radians. Additionally, a frequency of 1 Hz was used; one order of magnitude greater than the maximum frequency of the first seven numerical tests. Initial liquid distribution and temperature boundary conditions are shown in Figure 21.

The results of a sixty second run are shown in Figure 22. The sinusoidal motion of the liquid is evident. The overall volume of liquid in the groove is decreasing with time as evidenced by the maximum amplitude of the area peaks at $x^* = 0$ and $x^* = 1$ decreasing with time. No dryout is seen in the figure but this is only because the computer run was stopped before dryout occurred. The code appears to predict the correct trends in the liquid motion.



Run Parameters

$\Psi_{init} = 0\text{ rad}$	$\sigma = \text{on}$	$t_\infty = 10\text{ s}$
$\Psi_{max} = 0.0524\text{ rad}$	$\dot{m}_e = \text{on}$	$L_\infty = 0.254\text{ m}$
$\omega = 0.1\text{ Hz}$		

Figure 15. Numerical Test Five Parameters

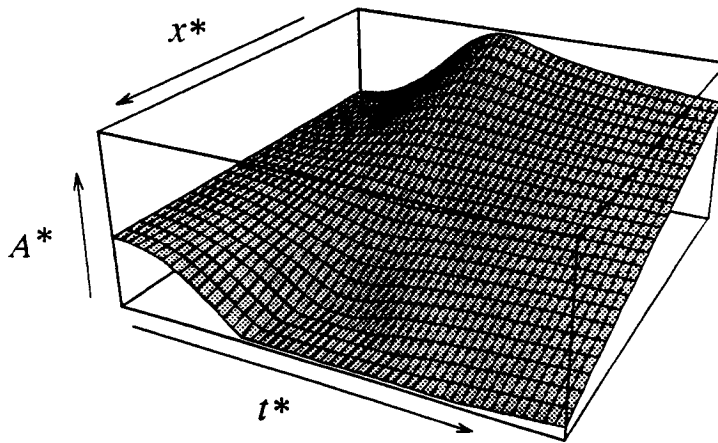
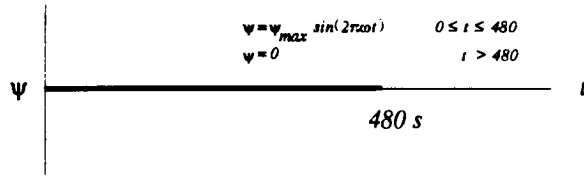
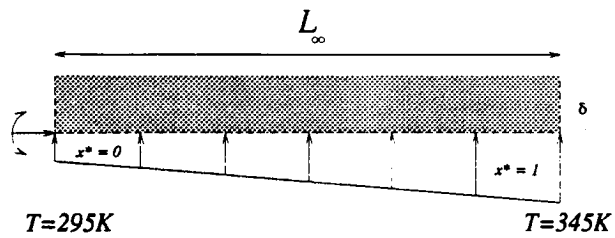


Figure 16. Numerical Test Five Results



Run Parameters

$\Psi_{init} = 0 \text{ rad}$	$\sigma = on$	$t_\infty = 480 \text{ s}$
$\Psi_{max} = 0 \text{ rad}$	$\dot{m}_e = on$	$L_\infty = 0.254 \text{ m}$
$\omega = 0 \text{ Hz}$		

Figure 17. Numerical Test Six Parameters

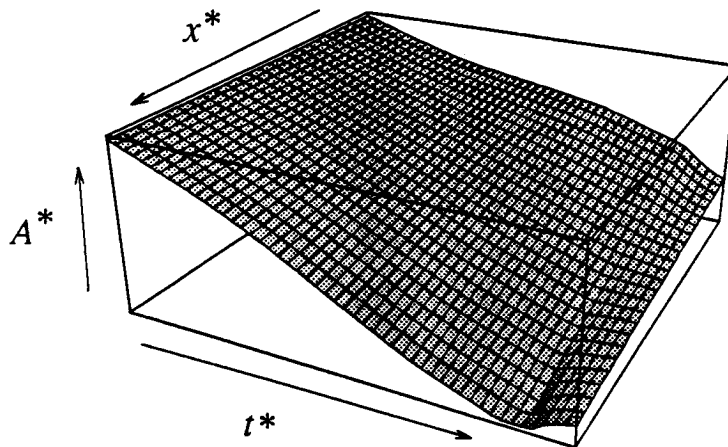
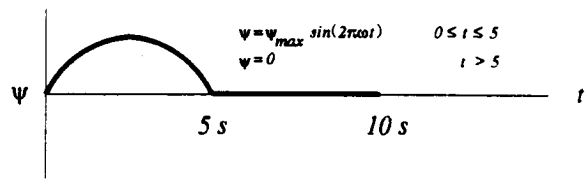
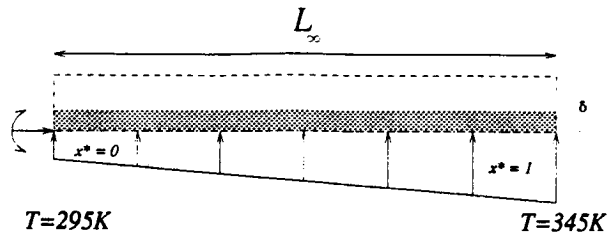


Figure 18. Numerical Test Six Results



Run Parameters

$\Psi_{init} = 0 \text{ rad}$	$\sigma = \text{on}$	$t_\infty = 10 \text{ s}$
$\Psi_{max} = 0.0524 \text{ rad}$	$\dot{m}_e = \text{on}$	$L_\infty = 0.254 \text{ m}$
$\omega = 0.1 \text{ Hz}$		

Figure 19. Numerical Test Seven Parameters

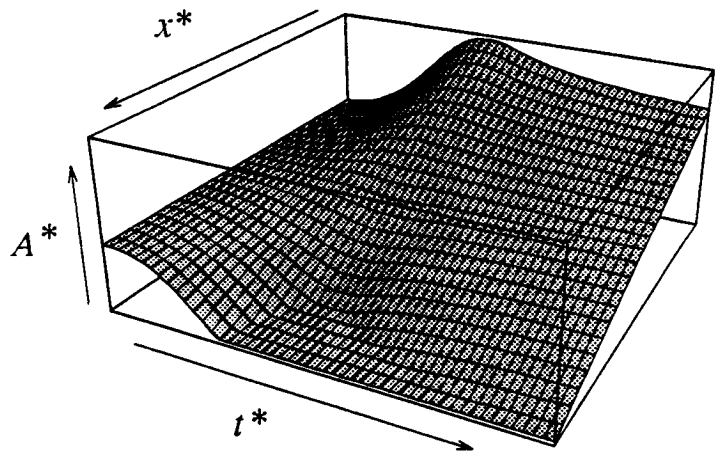
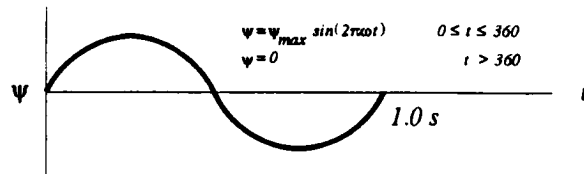
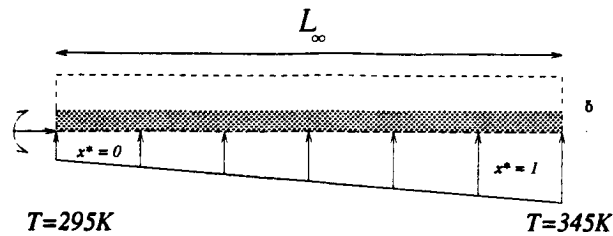


Figure 20. Numerical Test Seven Results



Run Parameters

$\Psi_{init} = 0 \text{ rad}$	$\sigma = \text{on}$	$t_\infty = 60 \text{ s}$
$\Psi_{max} = 0.0524 \text{ rad}$	$\dot{m}_e = \text{on}$	$L_\infty = 0.254 \text{ m}$
$\omega = 1.0 \text{ Hz}$		

Figure 21. Numerical Test Eight Parameters

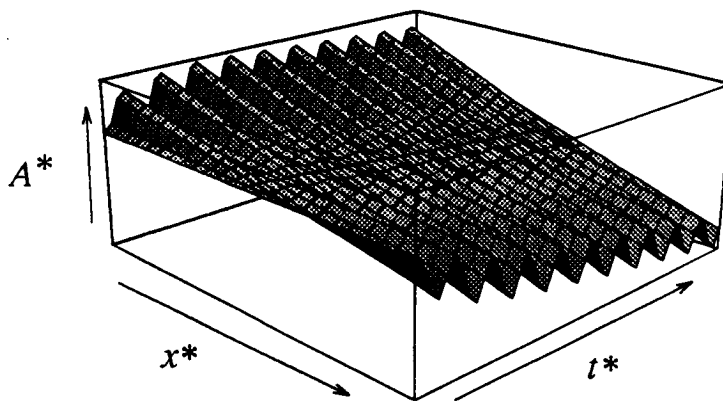


Figure 22. Numerical Test Eight Results

CONCLUSIONS AND RECOMMENDATIONS

A transient, one-dimensional numerical code has been developed which is capable of modeling the liquid motion in a grooved heat pipe wick structure subject to transient heat loads and body force effects. Simple numerical tests demonstrated its ability to predict the correct trends in axial variation of liquid inventory, to include both dryout and rewet, caused by asymmetric heating, transient body forces or a combination of both. It is recommended that experimental data be generated to compare with the results from this model to provide validation of the governing equations, simplifying assumptions and solution methodology.

REFERENCES

1. Peterson, G.P. "Heat Pipes in the Thermal Control of Electronic Components," *Proceedings of the 3rd International Heat Pipe Symposium*, Tsukuba City, Japan, Sep 1988.
2. Yerkes, K.L. and Hager, B.G., "Transient Response of Heat Pipes for Actuator Thermal Management," SAE Technical Paper Series 92-1024, Apr 1992.
3. Müller, R. "Analysis of the Liquid Distribution in Capillary Grooves of a SpacePlane Evaporation Cooler," *Proceedings of the 8th International Heat Pipe Conference*, Beijing, China, Sep 1992.
4. Jen, H. Summary Report for Axially Grooved Heat Pipe Study. contract NAS5-22562. Towson, Maryland: B & K Engineering, Inc., July 1979.
5. Beam, J.E. "Transient Heat Pipe Analysis," AIAA Paper 85-0936, Jun 1985.
6. Reagan, M.K. *Transient Body Force Effects on the Dryout and Rewet of a Heated Capillary Structure*. PhD Dissertation. Air Force Institute of Technology, Wright-Patterson AFB, OH, Apr 1994.
7. Hawthorne, Capt L.S. *Rewet Performance of a Rectangular Grooved Heat Pipe Wick After Gravitationally Induced Dryout*. MS Thesis. Air Force Institute of Technology, Wright-Patterson AFB OH, Dec 1993.
8. Shah, R.K. and London, A.L. "Laminar Flow Forced Convection in Ducts," Academic, New York, 1978, p. 190.
9. Chi, S.W. "Heat Pipe Theory and Practice," McGraw-Hill, Washington, 1976, pp. 40-41.
10. Kays, W.M. and Crawford, M.E. "Convective Heat and Mass Transfer." 2nd ed., McGraw-Hill, New York, 1987, p. 103.